3.

DESIGN AND ANALYSIS OF HIGHLY ISOLATED DUAL-BAND MIMO/DIVERSITY ANTENNA FOR MOBILE HANDSETS

3.1 Introduction

In today's fast paced world, MIMO technology made a great breakthrough by satisfying the demand of higher quality mobile communication services without using any additional radio resources [Vaughan and Anderson (1987), Foschini and Gans (1998)]. The huge potential of MIMO technique is evidenced by a rapid adoption into the wireless standards, such as WLAN, LTE, and WiMAX. Traditionally, MIMO systems employ multiple antenna elements to send or receive signals. In MIMO systems, mutual coupling is a well known effect and it becomes more critical when inter-element spacing is very small. This kind of situation can occur in mobile communications, especially in mobile phones, where space limitations become an important variable. In recent years, the interest of multiband, multi antenna systems have been growing for multi standard wireless terminals. In such multiband devices, achieving high isolation between the radiating elements is a challenging task and also it is difficult to control the isolation over the desired bands. So it gives a real challenge to antenna designers to produce an efficient MIMO system.

Some of the solutions reported in [Sonkki and Salonen (2010), Meshram *et al.* (2012), Chiu *et al.* (2007), Wu *et al.* (2003), Zhang *et al.* (2009), Weng *et al.* (2008), Makinen *et al.* (2007), Hsu *et al.* (2009), Diallo *et al.* (2006), Luxey *et al.* (2010), Chen *et al.* (2008)] to reduce the mutual coupling between two antenna elements. In [Sonkki and Salonen (2010), Meshram *et al.* (2012), Chiu *et al.* (2007), Wu *et al.* (2003), Zhang *et al.* (2009)], the mutual coupling was effectively reduced by using defected ground structures (DGS). Antenna array with low mutual coupling, operating at 2.45 GHz was reported in [Sonkki and Salonen (2010)], and the improvement of 40 dB isolation achieved by etching two

λ/2 slots on the ground plane. A combination of rectangular slot ring and inverted T-shaped slot stub was reported in [Meshram *et al.* (2012)] to reduce the mutual coupling between two quad band antennas. Ground plane with N-section resonator slots [Chiu *et al.* (2007)], protruded T-shaped ground plane [Wu *et al.* (2003)], and tree-like structure on ground plane [Zhang *et al.* (2009)] were implemented to improve port-to-port isolation. In [Weng *et al.* (2008)], transmission characteristics of different DGS and their equivalent circuit models were presented.

Electromagnetic band gap (EBG) structures, neutralization techniques, and lumped circuit networks are also attractive solutions to produce high isolation. Some of the EBG structures were reported in [Makinen *et al.* (2007), Hsu *et al.* (2009)] to reduce the mutual coupling by suppressing the surface waves. However, EBG structures require an intricate fabrication process and also a large area. Some of the neutralization techniques suggested in [Diallo *et al.* (2006), Luxey *et al.* (2010)] to improve isolation by utilizing a field cancelling concept. In [Diallo *et al.* (2006)] and [Luxey *et al.* (2010)], antennas were designed for the DCS and UMTS bands and studied the mutual coupling between them by considering the feeding strip facing and shorting strip facing cases. They used a single suspended line of different lengths for cancelling the fields and about -20 dB isolation was achieved. The lumped circuit networks presented in [Chen *et al.* (2008)] were used to provide good isolation of -23 dB between two antenna elements. But the lumped components induced the additional losses, which in turn strongly affect the total antenna efficiencies. So, even if MIMO system exhibits an acceptable isolation among multi antenna elements, it is necessary to decrease the antenna's mutual coupling to ensure that less power is lost in the other radiators and, thus, the total efficiencies are maximized.

In this chapter, a compact dual band PIFA for MIMO applications operating over the IEEE 802.11b/g (2.4 - 2.48 GHz) and IEEE 802.11a (5.15 - 5.85 GHz) bands is analyzed. Initially, the MIMO antenna system consists of two PIFAs. Each is constructed by E-shaped folded patch and with vertical parasitic strip.

This MIMO antenna system is producing acceptable isolation (≤ -15 dB) values by properly placing the antennas on the top corners of the PCB and selecting the positions of the feed points and shorting strips. However, when we place the mobile circuitry like battery, LCD, housing box, camera, sensors, acoustics, and other RF circuit elements around the antennas, there may be chance to deteriorate the isolation characteristics. Therefore, a MIMO antenna system with two folded shorting strips of 0.22λ at 2.45 GHz is proposed to achieve low mutual coupling to compensate the effect of mobile environment and improve the antenna efficiency, which helps to provide the better effective diversity gain. The folded shorting strip is connected between each antenna element (feed strip facing) and PCB ground plane. The idea is to create an additional coupling path such that the ground plane current from port 1 is not entering into port 2 so that a current loop is formed between shorting pin to feed point via folded shorting strip. Thus, the amount of current flowing from port 1 to port 2 is very negligible and it leads to low mutual coupling between two antenna elements.

3.2 Antenna Configuration and Design

The initial antenna structure shown in Fig. 3.1(a), consists of two symmetrical back-to-back PIFA elements, which are located on the top two corners of the substrate FR4 (PCB of mobile device with ε_r = 4.4 and tan δ = 0.018). The dimension of substrate is chosen as 100 × 60 × 0.8 mm^3 as mobile circuit board. The antenna element is made up of copper sheet with thickness of 0.2 mm. Fig. 3.1(b) shows the antenna structure with folded shorting strip, which is connected between each antenna element and ground plane. Fig. 3.2(a)-(c) show the details of single antenna element and its optimized dimension values.

The total lengths of the two radiating arms are chosen based on the fundamental PIFA resonant frequency (f_0) which is given as [Ogawa and Uwano (1994)].

$$f_0 = \frac{c}{4*(L_1+L_2)} \tag{3.1}$$

where, c is velocity of light, L_1 and L_2 are the length and width of the PIFA.

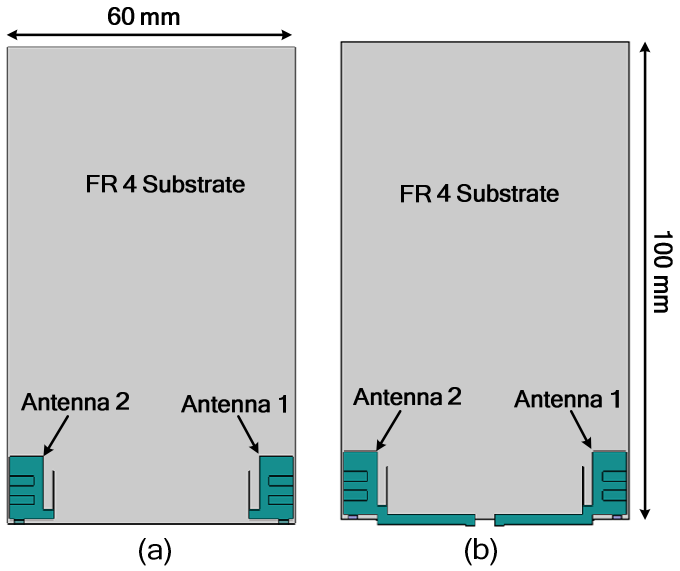

Figure 3.1: Proposed antenna (a) without folded shorting strip, and (b) with folded shorting strip.

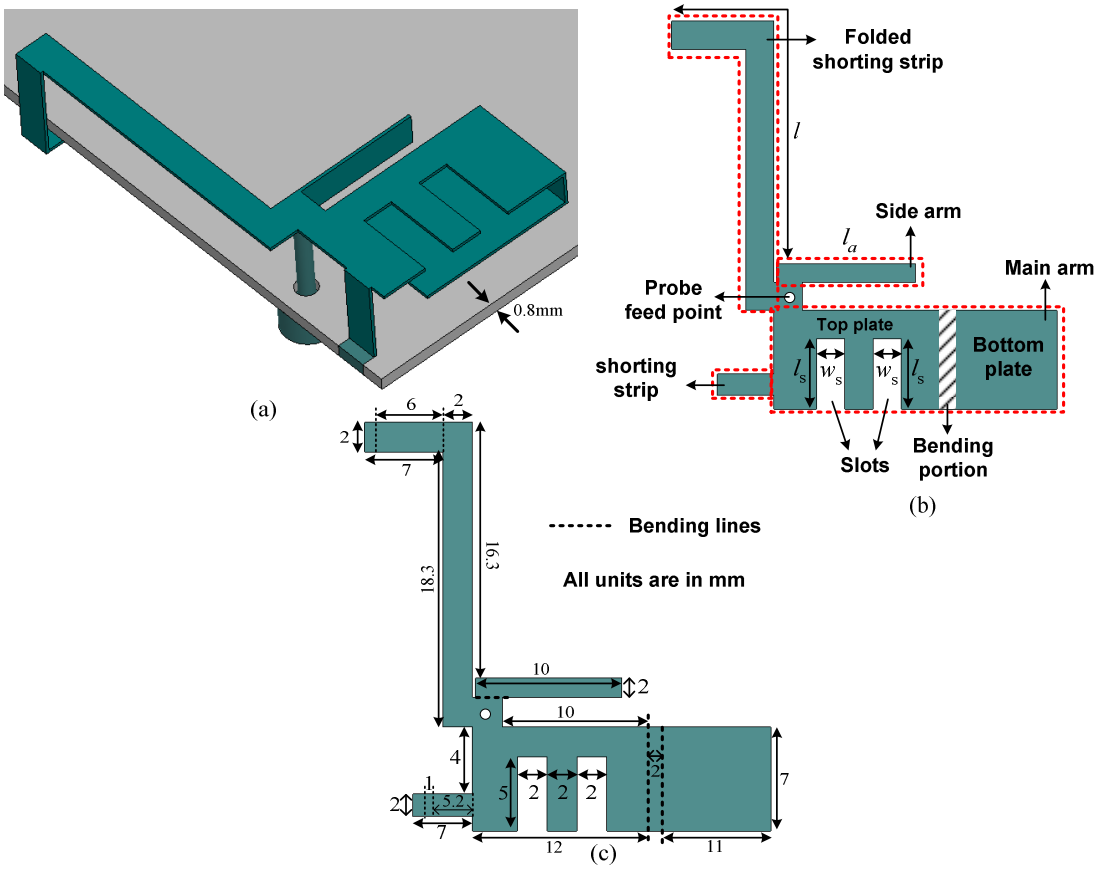

Figure 3.2:(a) 3-D view of single antenna element, (b) Unfolded planar structure of single antenna element, and (c) Optimized dimensions of (b) in mm.

Each radiating element comprises of two radiating arms namely, main arm and side arm which resonates at 2.45 GHz and 5.5 GHz frequencies, respectively. The length of the arm is chosen corresponding to $\lambda/4$ at resonating frequencies. Initially, only folded patch are considered i.e. without slot on the top of the patch and side arm. By taking into account of mobile space, the main radiating arm is folded and it resonates at 2.7 GHz and 7.1 GHz as shown in Fig. 3.3(a). In order to resonate at desired frequency (2.45 GHz), two slots are incorporated on the top patch plate. These two slots increase the electrical length of radiator and decrease the resonant frequencies from 2.7 to 2.45 GHz and 7.1 to 6.8 GHz as shown in Fig. 3.3(a). It is noted that, the higher frequency band is not properly tuned as well as not of our practical interest. Therefore, to achieve another desired frequency band which resonates at 5.5 GHz i.e., HiperLAN band, the side arm of length $\approx \lambda/4$ at 5.5 GHz is added to the main radiating element. The side radiating arm is bent vertically along to main arm so as to occupy less space in such a way that the compactness of antenna element remains within $12 \times 9 \times 6$ mm^3. After the addition of side arm, antenna resonates at 2.5 GHz and 5.5 GHz, resulting in the desired frequency bands.

Also, the simulated *S*-parameters (reflection and coupling) with and without folded shorting strip are plotted in Fig. 3.3(b). It is observed that without shorting strip the obtained isolation (S_{21}) values are better than -18 dB over 2.45 GHz band (2.4-2.485 GHz) and less than -15 dB over 5.5 GHz band (5.15-5.85 GHz). Though, these isolation values are acceptable (≤ -15 dB), when we implement this structure in practical mobile environment (LCD, battery and other RF circuits) there may be a chance to degrade the isolation characteristics and that causes to reduce the antenna total efficiency. In view of this, subsequent structure shown in Fig. 3.1(b) is proposed, which employs a folded shorting strip to reduce the surface current flow between two antenna elements on ground plane. The main role of folded shorting strip is to make a current loop to avoid the current flow from port1 to port2 so that we can achieve low mutual coupling. The current loop starts from shorting strip and next to ground plane and next to folded shorting

strip and towards feed point. The optimized length of the folded shorting strip is 0.22λ at 2.45 GHz. The achieved isolation values with proposed structure are below -28 dB over all operating frequency bands. The enhancement in isolation is 10 dB at 2.45 GHz band and 13 dB at 5.5 GHz band is observed. To further investigate the mechanism of the folded shorting strip, the surface current distribution and surface current vector plots at different frequency bands are depicted in the upfront section.

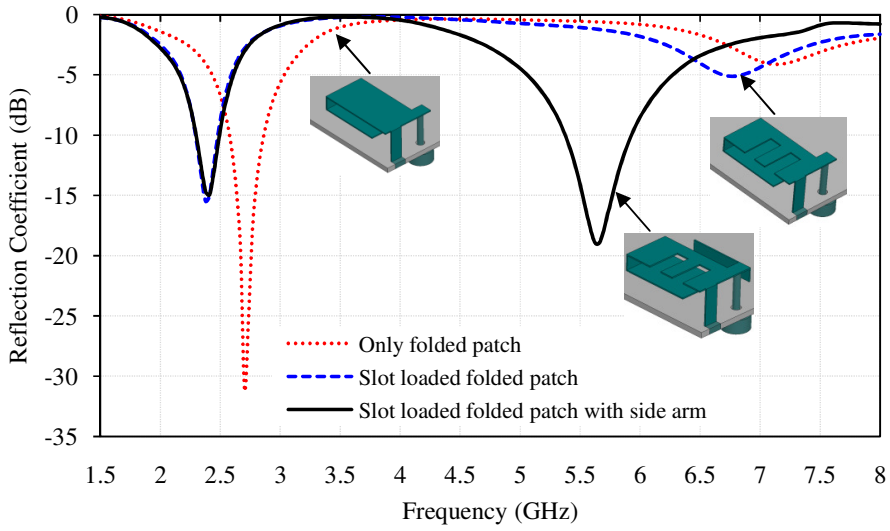

(a)

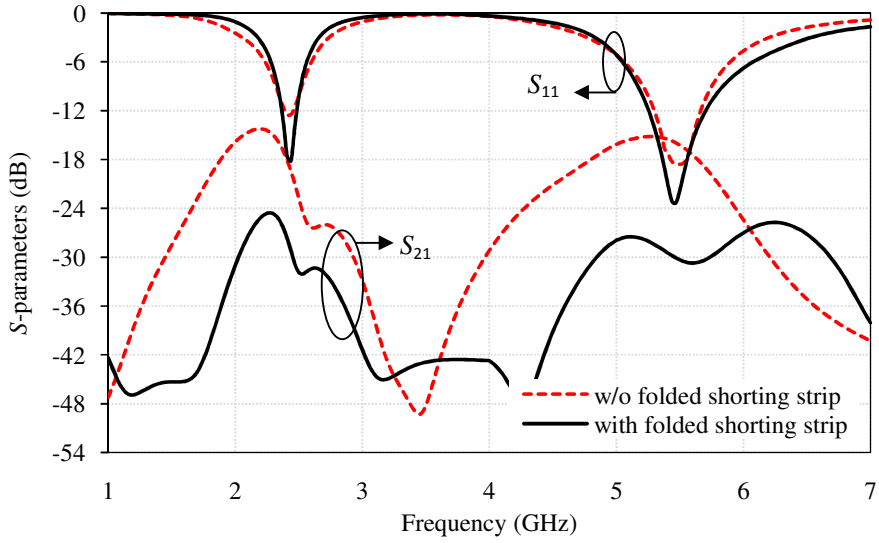

(b)

Figure 3.3: (a) Effect of different configurations on reflection coefficient, and (b) Effect of folded shorting strip on *S*-parameters.

3.3 Results and Discussion

All the simulations are carried out on Ansoft's High Frequency Structure Simulator (HFSS) software. Computer Simulation Technology Microwave Studio (CST MWS) is used to verify the HFSS result before going to fabricate the antenna. Further, CST MWS is used to calculate the radiation and diversity performances of the MIMO antenna. The detail descriptions of HFSS and CST MWS are given in Appendix I.

3.3.1 *S*-parameters and Radiation Performances

3.3.1.1 Parametric Analysis

The simulated results for *S*-parameters of the proposed structure with different slot length (l_s) are shown in Fig. 3.4(a). It is observed that the lower resonant frequency decreases with increase of slot length l_s. This is due to the fact that the electrical length of main radiating arm increases with l_s. In the upper band the effect of l_s is negligible and the optimized value of l_s is 5 mm. Fig. 3.4(b) shows the *S*-parameters for different slot width (w_s) by keeping l_s at 5 mm. The lower band is shifted towards higher frequency while decreasing w_s, and higher band is almost independent of w_s. The reason for frequency shifting is same as l_s. The isolation remains almost same for higher band and decreases at lower frequencies. The optimized value for w_s is obtained to be 2 mm. The *S*-parameters versus frequency for various values of side arm length (l_a) is shown in Fig. 3.4(c). By fixing the side arm width at 2 mm, the parameter l_a is tuned. It is observed that higher resonant frequency decreases with increase of length l_a and there is no significant effect on the isolation. At the lower band, the effect of side arm length on reflection and coupling *S*-parameters is completely insignificant. Fig. 3.4(d) shows the simulated reflection and coupling *S*-parameters of proposed structure with folded shorting strip length (l) as a variable. The length of folded shorting strip varies from 0.15λ to 0.24λ, where λ is lower resonating frequency at 2.45 GHz. It is observed that when the length of folded strip is 19 mm (0.15λ) then reflection coefficient becomes distorted at higher frequency due to the resonating

behaviour of the folded strip whereas on other values like 0.22λ and 0.24λ, insignificant effect on reflection coefficient whereas the coupling parameter improved almost from -23dB to -29dB.

3.3.1.2 Simulated and Measured *S*-parameters

Fig. 3.5(a) shows the fabricated antenna and size compared with Samsung Galaxy S GT I9000. The *S*-parameters of the fabricated antenna are measured by Agilent Technology (E8364B, 10 MHz–50 GHz) Network Analyzer. The simulated and measured reflection and coupling *S*-parameters of the MIMO antenna are shown in Fig. 3.5(b).

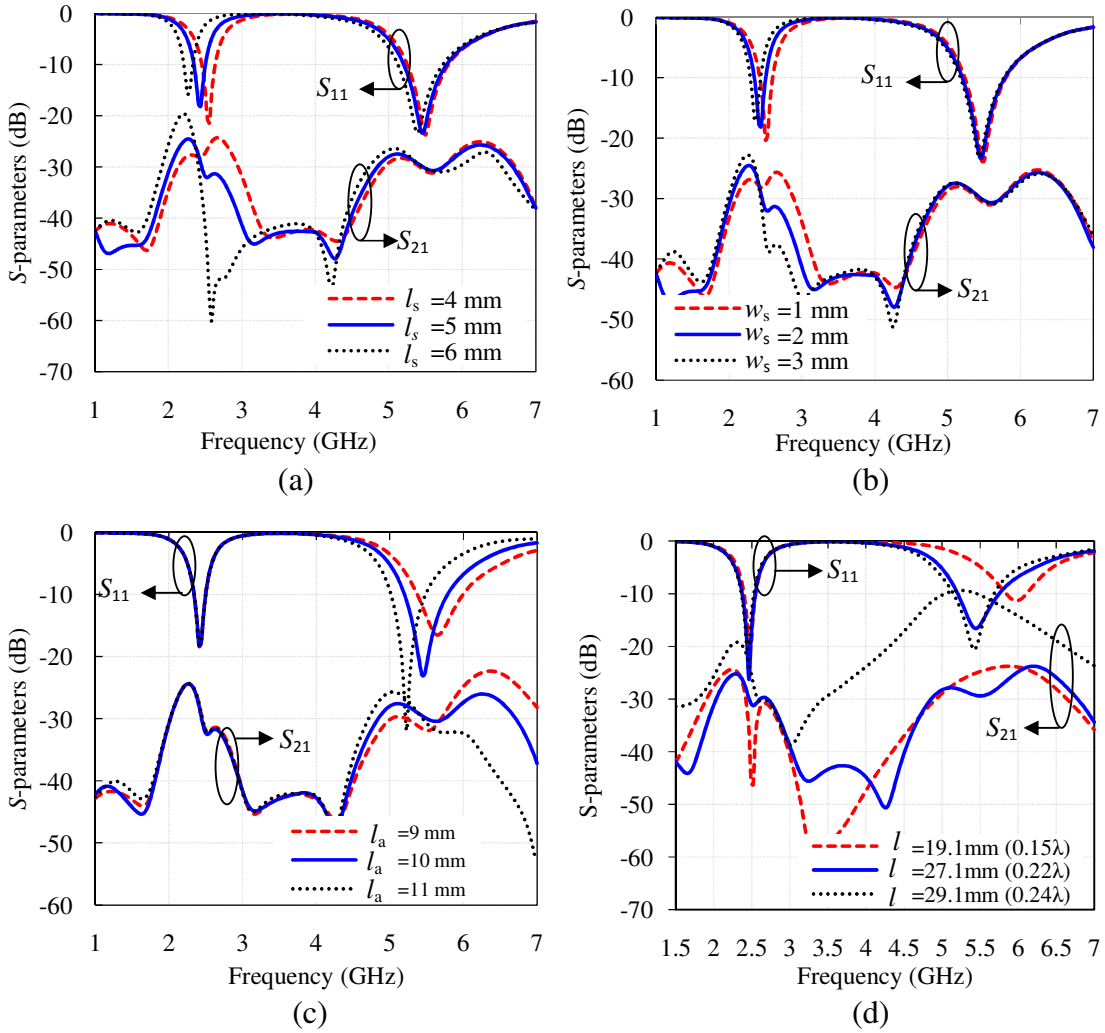

Figure 3.4: Variation of *S*-parameters with (a) slot length (l_s), (b) slot width (w_s), (c) side arm length (l_a), and (d) folded shorting strip length (l).

The measured bandwidth of 290 MHz (2.39-2.68 GHz, 11.4%, VSWR 2.33:1 or -6 dB reflection coefficient) at WLAN (IEEE 802.11b/g) band and 1150 MHz (4.85- 6 GHz, 21.2%, VSWR 2.33:1 or -6 dB reflection coefficient) at WLAN (IEEE 802.11a) band is achieved [Zhang (2011)]. The isolation (S_{21}) values are below -28 dB and -26 dB (-30 dB most of the band) respectively over the aforementioned WLAN bands. This means that the folded shorting strip is providing excellent isolation values by cutting down the surface current flow on ground plane between two antenna elements.

3.3.1.3 Radiation Performances

The simulated 3D and measured 2D radiation patterns of the proposed MIMO antenna in free space at 2.45 GHz and 5.5 GHz are shown in Fig. 3.6(a) and Fig. 3.6(b), respectively. The simulated as well as measured radiation patterns are obtained by exciting a single port at a time and matched terminated to other port. The measured radiation patterns are plotted in two planes i.e., horizontal plane (Theta=90^0) and vertical plane (Phi=90^0). It is illustrated that the simulated and measured radiation patterns of the two antenna elements point to complimentary

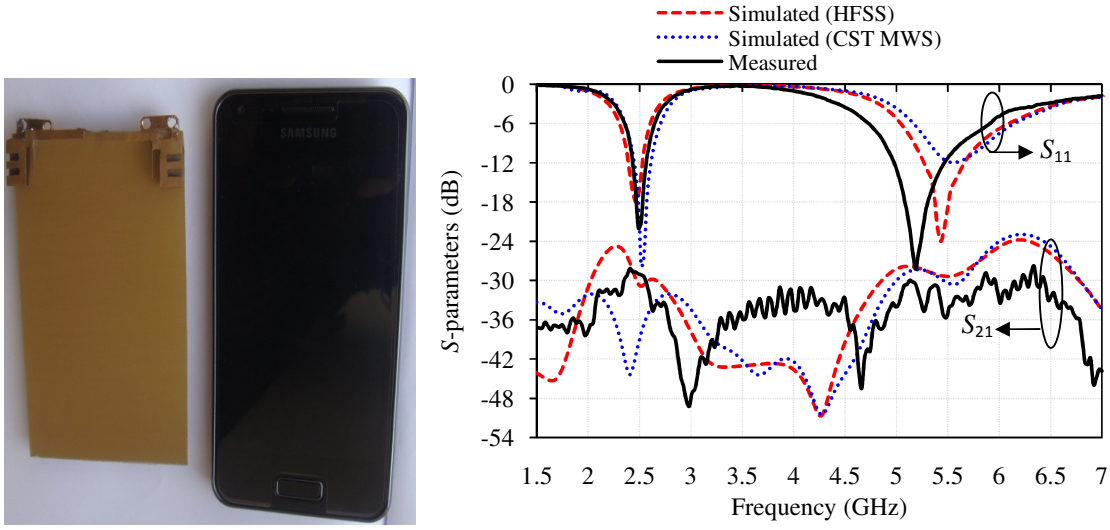

(a) (b)

Figure 3.5: (a) Prototype of proposed antenna (size compared with Samsung Galaxy S GT I9000), and (b) Simulated and measured *S*-parameters of proposed structure.

spatial region which shows pattern diversity criterion of the proposed MIMO antenna and this property can provide low correlation and good antenna diversity in free space.

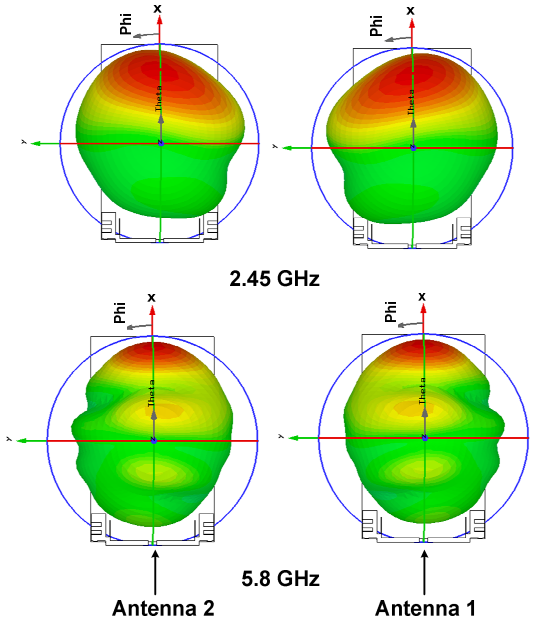

(a)

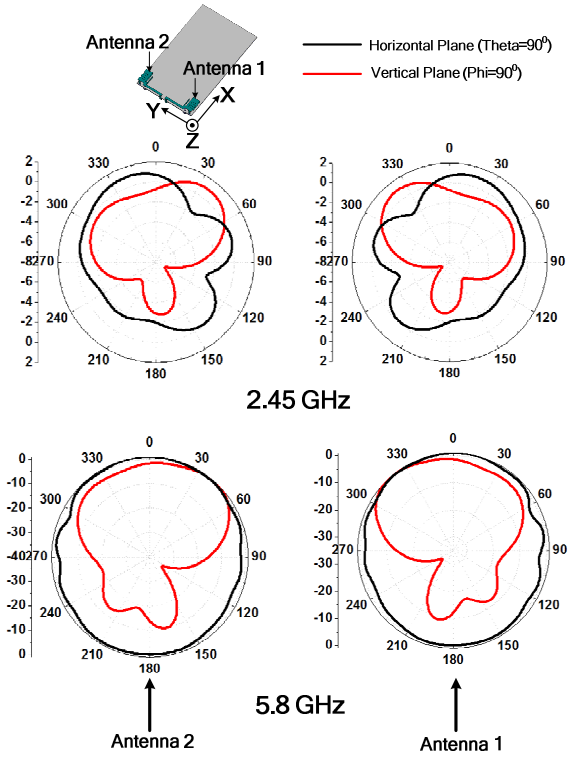

(b)

Figure 3.6: Far field radiation patterns (a) Simulated 3D at 2.45 GHz and 5.5 GHz, and (b) Measured 2D at 2.45 GHz and 5.5 GHz.

The measured peak realized gain and calculated total antenna efficiency of the proposed MIMO antenna are shown in Fig. 3.7. In MIMO antenna system each antenna elements are placed symmetrical on the PCB of mobile circuit board. The peak realized gain and total antenna efficiency of each elements (Antenna 1 and Antenna 2) are equal. The total antenna efficiency is calculated by considering the antenna mismatch losses [Balanis (2005)]. It is found that the calculated total antenna efficiency is varies from 55% to 87% in WLAN band (IEEE 802.11b/g) and 80% to 89% at WLAN band (IEEE 802.11a). The measured peak realized gain varies from 4.5dBi to 4.8dBi in WLAN band (IEEE 802.11b/g) and 6.8dBi to 7.2dBi in WLAN band (IEEE 802.11a).

3.3.2 Surface Current Distribution

The effect of the folded shorting strip is clearly noticed in the surface current distribution plots as shown in Fig. 3.8(a)-(b). These all plots are taken out when Antenna1 is excited and Antenna2 is matched terminated. For without folded shorting strip structure a small amount of surface current is coupled from Antenna1 to Antenna2 through common ground plane. This surface current flow between two ports is reduced to a great extent by the folded shorting strip at all above mentioned frequencies and also the effect is same when Antenna2 is excited and Antenna1 is matched terminated. From the Fig. 3.8(c)-(d) it is clearly shown that very less amount of current is flowing towards port2 and maximum amount of ground current is flowing into folded shorting strip and towards feed point. So the folded shorting strip can significantly increase the isolation of MIMO antenna system.

3.3.3 Diversity Parameters Analysis

All the diversity parameters (ECC, MEG, and EDG) of proposed dual-band highly isolated MIMO antenna are demonstrated using CST MWS.

3.3.3.1 Envelope Correlation Coefficient (ECC)

To calculate ECC, far field pattern data method is used which has already been discussed in previous chapter. The calculated values of ECC of the proposed

MIMO antenna are shown in Fig. 3.9. It is observed that the values of ECC are well below within the allowable limit of 0.5 for the proposed dual band MIMO antenna system.

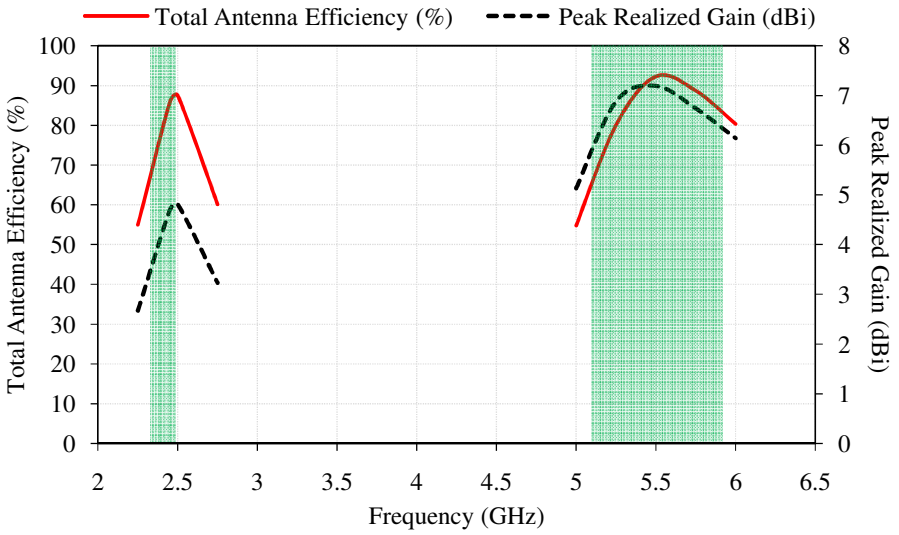

Figure 3.7: Variation of measured peak realized gain and calculated total antenna efficiency.

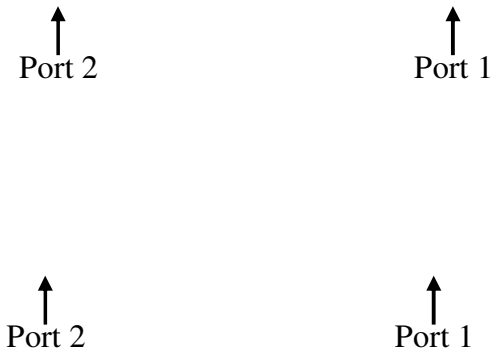

Figure 3.8: (a) Surface current distribution at 2.45 GHz, (b) Surface current distribution at 5.5 GHz, (c) Vector surface current flow on folded shorting strip at 2.45 GHz, and (d) Vector surface current flow on folded shorting strip at 5.5 GHz.

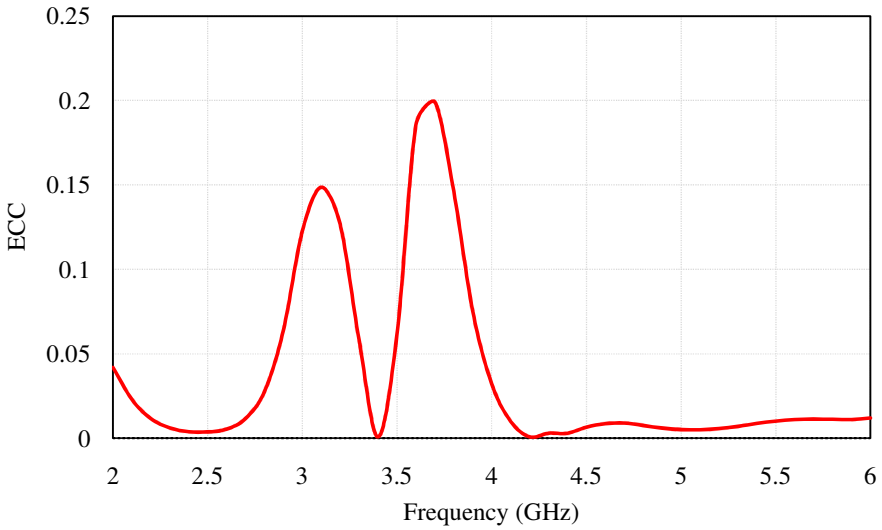

Figure 3.9: Variation of ECC with frequency.

3.3.3.2 Mean Effective Gain (MEG)

The MEG of a MIMO antenna system is calculated by the formula discussed in previous chapter [Taga (1990)]. For the case of mobile user, it is quite logical to assume that when a mobile user moves randomly in any environment, the incident waves can arise from any azimuth direction with equal probability.

However, such an assumption can not be made in elevation direction. A few models have been presented in [Taga (1990)], [Dong *et al.* (2002)]. The distributions of the angular density functions depend on the surrounding environment. Some sample statistical models and their typical parameter values for indoor, outdoor, and isotropic environments have been discussed for the angular density functions in [Karaboikis *et al.* (2008)].

Table 3.1 gives the computed MEG in free space for different *XPR* at different resonating frequencies by setting the, $m_v = 10^0$, $m_H = 10^0$ and $\sigma_v = 15^0$, $\sigma_H = 15^0$. The MEG of Antenna 1 and Antenna 2 are indicated as MEG1 and MEG2, respectively. From the Table 3.1, it is observed that the ratio of the MEG1/MEG2 is close to unity which satisfies the equality criterion of the two antennas.

3.3.3.3 Effective Diversity Gain (EDG)

In this section, the effect of folded shorting strip can be seen on the total antenna efficiency and EDG. The EDG is directly related with the efficiency and ECC. EDG can be calculated by apparent diversity gain (G_{app}). The relation between apparent diversity gain and correlation coefficient are discussed in previous chapter [Schwarts *et al.* (1965)]. The impact of folded shorting strip on total efficiency is clearly noticeable from Table 3.2. The average improvement of 10% in total efficiency over the desired bands is due to the fact that the folded shorting strip structure provides good matching conditions to PIFA and also producing the good reflection and isolation characteristics compared to without folded shorting strip structure. The EDG of MIMO antenna system is determined by multiplying the diversity gain with total antenna efficiency. From the Table 3.2, it is clearly observed that the folded shorting strip structure brings the improvement of 1dB in EDG.

Table 3.1: Computed MEGs at different resonating frequencies for different XPRs.

Freq. (GHz)	Indoor (XPR=5 dB)		Outdoor (XPR=1 dB)		Isotropic (XPR=0 dB)	
	MEG1	MEG2	MEG1	MEG2	MEG1	MEG2
2.45	-6.015	-6.150	-5.367	-5.412	-5.2	-5.2
	MEG1/MEG2 0.98		MEG1/MEG2 0.99		MEG1/MEG2 1	
5.25	-3.189	-3.190	-3.796	-3.896	-3.985	-3.85
	MEG1/MEG1 0.99		MEG1/MEG1 0.97		MEG1/MEG1 1.04	
5.5	-3.184	-3.185	-3.805	-3.812	-3.996	-3.981
	MEG1/MEG2 0.99		MEG1/MEG2 0.99		MEG1/MEG2 1.004	
5.8	-3.048	-3.150	-3.706	-3.720	-3.911	-3.950
	MEG1/MEG2 0.97		MEG1/MEG2 0.99		MEG1/MEG2 0.99	

Table 3.2: The effect of folded shorting strip on diversity gain, and effective diversity gain.

Freq. (GHz)	Without folded shorting strip			With folded shorting strip		
	DG (dB)	$\eta_{total}(\%)$	EDG (dB)	DG (dB)	$\eta_{total}(\%)$	EDG (dB)
2.45	9.997	78.0	7.79	9.999	86.0	8.60
5.25	9.996	79.0	7.89	9.999	90.4	9.04
5.5	9.999	90.0	8.99	9.999	99.0	9.89
5.8	9.999	81.6	8.15	9.999	91.0	9.09

3.3.4 Analysis of MIMO Antenna in Actual Mobile Scenario

Fig. 3.10 shows the typical environment of a mobile phone. The mobile environment consists of a large size touch screen LCD, a battery, a camera (diameter 8.5 mm and thickness 6 mm), and a speaker. The position of speaker is opposite side to the camera with dimension of 8.5 mm width and 18 mm length, respectively. A large size LCD of volume 73 × 47 × 2 mm^3 and a battery of volume 65×47×3 mm^3 are settled parallel with a spacing of 1 mm and are connected with the main PCB via connectors. All these components are assumed as Prefect Electric Conductor (PEC) during the simulation. In addition to this, the small metallic components like three buttons and one microphone are also considered which are far from the antenna elements. All these components and antenna elements are covered with a 1 mm thick plastic box of dielectric constant 3 and conductivity 0.02 S/m which form housing of the mobile phone.

Fig. 3.11 shows the variation of the *S*-parameters of the MIMO antenna. In the presence of mobile environment, the slight variation in higher resonance frequency is observed but desired operating frequency band based on -6 dB reflection coefficient is covered. The isolation between the two antennas is still maintained at -22 dB over all the operating bands.

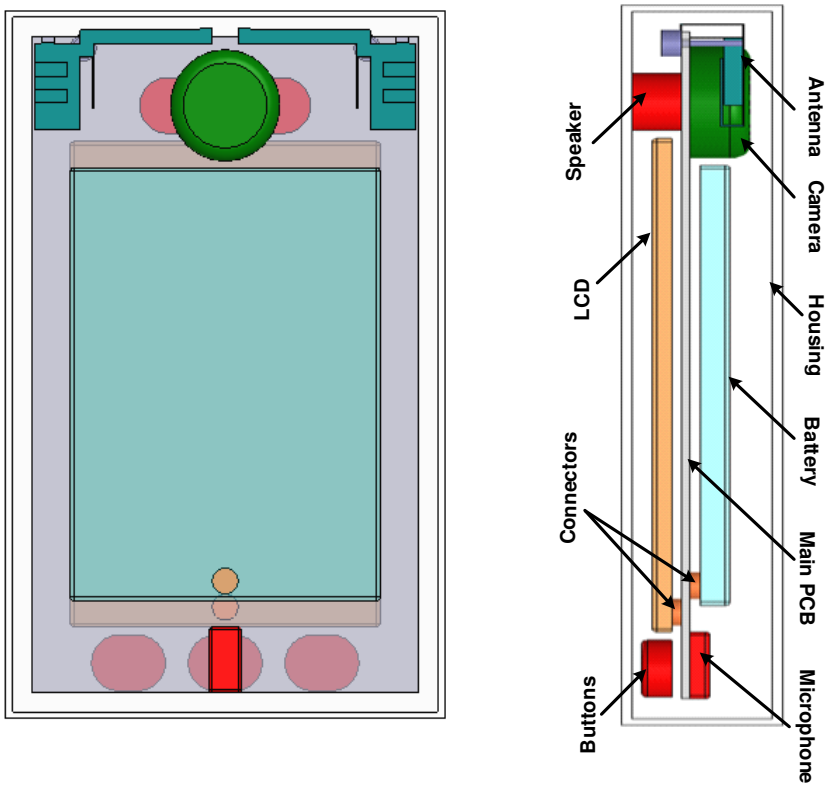

Figure 3.10: Configuration of mobile environment with MIMO antenna.

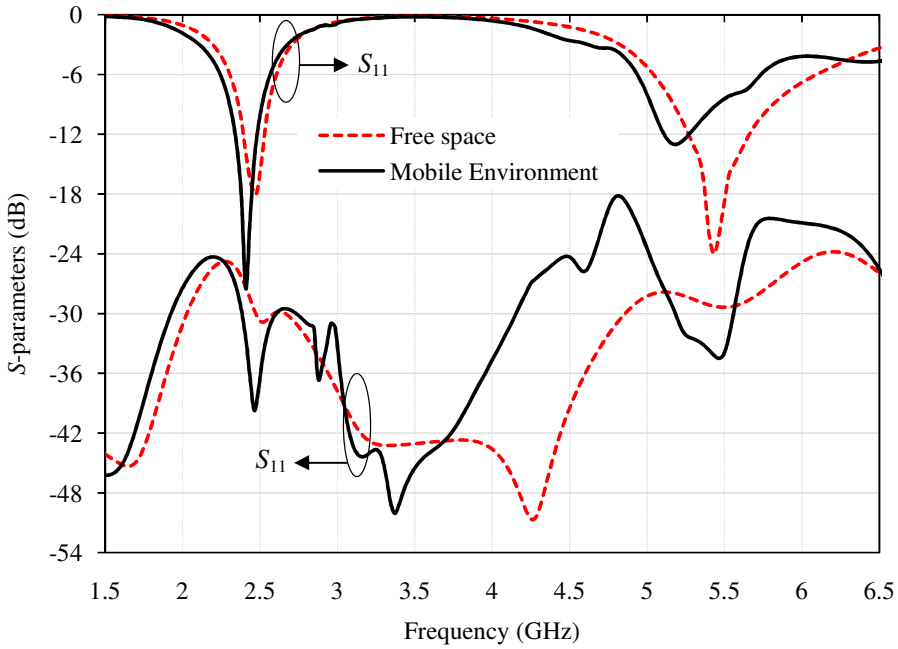

Figure 3.11: Effect of mobile environment on *S*-parameters of MIMO antenna.

In the present scenario, the evoluation of mobile phone is rapidly growing so the electromagnetic radiation and absorption on human body has become an important issue. Due to the extensive spread of mobile handsets, the radiations of mobile phones have rapidly been increased attention. The electromagnetic radiation in human tissues can be evaluated by SAR, which represents the time rate of microwave energy absorption inside the tissue [Durney *et al.* (1986)].

The MIMO antenna system will be mounted on the mobile phones soon, which will bring new problem for evaluating the antenna's SAR. Unlike a single antenna system, in the MIMO antenna system one antenna will interact with other antenna and this interaction will change the SAR performance of each other. In MIMO system, the antennas might operate simultaneously to achieve the high data rate and low correlation. From Federal Communication Commission (FCC) standard [FCC Report (2008)], SAR to PEAK Location Spacing Ratio (SPLSR) is utilized to evaluate the SAR performance when dual antenna element operates simultaneously and given as:

$$SPLSR = (SAR1+SAR2)/D \tag{3.2}$$

where, SAR1 and SAR2 are the SAR value of Antenna 1 and Antenna 2, respectively, D is the separation between two SAR peaks in centimetres. In this analysis, the position of mobile phone (antenna with mobile environment is shown in Fig. 3.10) near to the human head phantom are placed according to the CTIA standard [CTIA Report (2005)] and shown in Fig 3.12. The incident power for SAR evaluation is 21dBm (0.125W) at 2.45 GHz [FCC Report (2007)] while the incident power is 17dBm (0.05W) at 5.5 GHz [Saidatul *et al.* (2009)]. The distribution of electromagnetic energy inside human tissues is shown in Fig. 3.12. Table 3.3 listed the simulated 1g and 10g average SPLSRs at the frequencies 2.45 GHz and 5.5GHz of WLAN bands. It is observed that the calculated values of SPLSR meet the standard of FCC.

In the case of multi element MIMO system, the TRP is calculated for each elements named as TRP1 and TRP2 of Antenna 1 and Antenna 2, respectively. The TRPs are calculated in free space as well as in user proximity and given in

Table 3.4. It is observed that in the case of free space, TRP of Antenna 1 and Antenna 2 are same due to the uniform environment around the MIMO antenna elements. Due to the low reflection loss and high total efficiency, the TRPs in free space is high i.e. more than 26 dBm. When we implement proposed antenna in real scenario, the TRP decreases due to the large human body coverage around antenna elements but still better than 24 dBm.

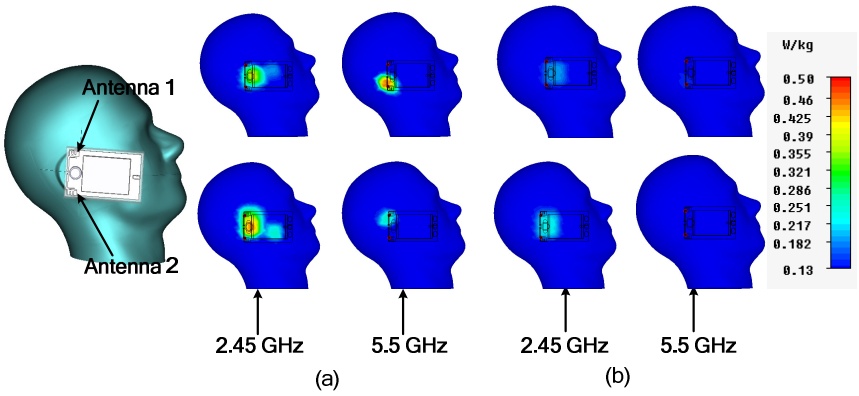

Figure 3.12: Distribution of energy over human head phantom, (a) Average SAR over 1g and (b) Average SAR over 10g.

Table 3.3: SAR performances of MIMO antenna on human head.

Distribution of SAR over 1g tissue					Distribution of SAR over 10g tissue			
Freq. (GHz)	SAR_1 (W/kg)	SAR_2 (W/kg)	Separation distance b/w SAR peaks (D) unit in centimetre (cm)	SPLSR $= \frac{(SAR_1 + SAR_2)}{D}$ (W/kg/cm)	SAR_1 (W/kg)	SAR_2 (W/kg)	Separation distance b/w SAR peaks (D) unit in centimetre (cm)	SPLSR $= \frac{(SAR_1 + SAR_2)}{D}$ (W/kg/cm)
2.45	0.37	0.44	3.26	0.25	0.188	0.227	1.9	0.22
5.5	0.46	0.254	2.92	0.24	0.14	0.075	2.7	0.08

Table 3.4: Calculated values of TRP in free space and user proximity.

Frequency (GHz)	Free Space		User Proximity	
	TRP1 (dBm)	TRP2 (dBm)	TRP1 (dBm)	TRP2 (dBm)
2.45	26.3	26.3	25.2	24.8
5.5	26.6	26.6	24.9	24.8

3.4 Summary

In this chapter, a compact dual band MIMO antenna with low mutual coupling operating over WLAN bands (2.4-2.485 GHz and 5.15-5.85 GHz) is studied. The measured 6dB return loss bandwidths are 510 MHz and 1700 MHz over lower and higher resonating frequencies, respectively. Excellent isolation is achieved between two antenna elements by folded shorting strip. The antenna total efficiencies are improved 10% average over the operating frequency bands, and also the improved isolation values are less than -28 dB at WLAN (IEEE 802.11.b/g) band and better than -26 dB (-30 dB in most of the band) across WLAN (IEEE 802.11a) band. The radiation patterns of two antennas are providing good pattern diversity characteristics and also obtained excellent ECC (lower than 0.01), well diversity gains and the satisfactory MEG ratio over the frequency of interested bands. The performance of the proposed antenna in the user proximity shows practical application for mobile handset applications. The calculated values of SPLSR are well below the defined FCC limit. All above attributes of the proposed antenna makes it suitable for mobile handset applications.

After the investigations of dual-band MIMO/Diversity antenna for WLAN applications, the miniaturized triple band MIMO diversity antenna for WLAN, WiMAX, and HiperLAN applications is taken up in the chapter four.